JCTC Journal of Chemical Theory and Computation

Article

pubs.acs.org/JCTC

# Improved Predictor−Corrector Integrators For Evaluating Reaction Path Curvature

Hrant P. Hratchian*,† and Elfi Kraka*,‡

†Gaussian, Inc., 340 Quinnipiac Street, Building 40, Wallingford, Connecticut 06492, United States

‡Department of Chemistry, Southern Methodist University, 3215 Daniel Avenue, Dallas, Texas 75275, United States

**ABSTRACT:** The reaction *path* connects a chemical potential energy landscape and the conceptual descriptions of chemical mechanisms and reactivity. In recent years, a class of predictor−corrector integrators has been developed and shown to provide an excellent compromise between computational efficiency and numerical accuracy. Models based on projected frequencies along the reaction path and coupling matrix elements, such as Reaction Path Hamiltonian (RPH) and Unified Reaction Valley Approach (URVA), require highly accurate integration of the reaction path. In this report, the Euler Predictor−Corrector (EulerPC) and Hessian-based Predictor−Corrector (HPC) methods are shown to be *inadequate* for studying reaction path curvature, which is a central component of the RPH and URVA models. The source of this apparent failure is explored, and a solution is developed. Importantly, the resulting enhanced EulerPC and HPC integrators do not require more intensive CPU or memory requirements than their predecessors.

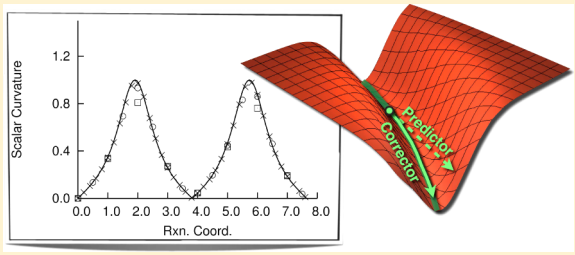


## 1. INTRODUCTION

Accurate integration of the steepest-descent reaction pathway is the critical first step in nearly all mechanistic and kinetics models based on the transition state theory.[1,2] Perhaps the most widely−used reaction pathway definition is Fukui's intrinsic reaction coordinate (IRC).[3] The IRC is the steepest-descent path initiated at the transition structure (TS), a first-order saddle-point on the potential energy surface (PES), by stepping forward and backward along the Hessian eigenvector corresponding to the imaginary frequency. The pathway is followed in mass-weighted Cartesian coordinates. As a function of the reaction coordinate $s$, the atomic positions $\mathbf{x}(s)$ are propagated according to

$$\frac{d\mathbf{x}}{ds} = -\frac{\mathbf{g}(\mathbf{x})}{|\mathbf{g}(\mathbf{x})|} \tag{1}$$

where $\mathbf{g}(\mathbf{x})$ is the energy gradient at $\mathbf{x}$. Despite the conceptual simplicity of eq 1, it can exhibit stiff character and be difficult to integrate in regions of the path where the gradient is small.

In quantum chemistry applications, reaction path based methods can be readily employed with model chemistries for which analytic energy derivatives are available. For such work, the choice of an integrator must carefully balance cost and accuracy considerations. As a result, a number of specialized methods have been developed.[4−31] Among these, the integrator of Hratchian and Schlegel and the related method of Hratchian and co-workers have been shown to provide an excellent cost/accuracy balance for examinations of energy and coordinate profiles along the reaction path.[28−31] In general, these integrators provide an accuracy similar to the widely used second-order implicit method of Gonzalez and Schlegel (GS2),[24,25] while also being 2 to 5 times less computationally expensive.

Recently, it was shown that HPC and EulerPC integrators provide reaction pathways accurately enough to produce excellent projected frequency profiles for a particularly challenging reaction.[32] This degree of accuracy is necessary if one is to use an IRC for evaluating a rate constant using the well-known variational transition state theory (VTST) approach.[33−35] For reaction path Hamiltonian (RPH) and related models, it is further necessary to evaluate the reaction path curvature and coupling matrix elements.[36] One such method is the Unified Reaction Valley Approach (URVA) of Kraka and co-workers.[37−39] URVA uses the reaction path curvature and its decomposition into curvature coupling elements to provide a detailed mechanistic account.

In previous quantum chemistry based URVA investigations, the IRC integration using the GS2 method has represented a significant component of the total computational effort. Given the success of HPC and EulerPC for evaluating projected frequency profiles, it seems reasonable to apply these methods in URVA studies. In this way, one would hope to decrease the IRC expense by as much as 75%. Disappointingly, preliminary work clearly showed that HPC and EulerPC integrators fall flat in the evaluation of reaction path curvature.

Figure 1 displays the scalar curvature (see below for a full definition) along the IRC for the rearrangement reaction HNC → HCN computed at the B3LYP/6-31G(d,p) level of theory.[40−44] The figure includes reference results from an

Received: November 20, 2012
Published: January 10, 2013

  

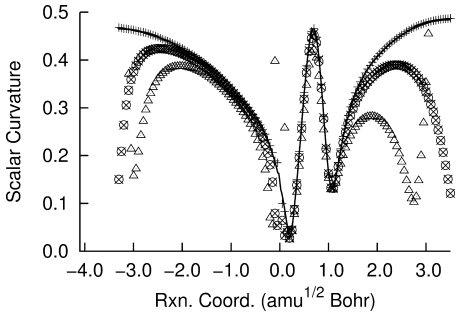


**Figure 1.** The scalar curvature as a function of reaction coordinate for the HCN → HNC rearrangement reaction comparing GS2 (+), LQA (Δ), EulerPC (×), and HPC (○) reaction path integration methods. A numerical integration step size of 0.05 amu$^{1/2}$ Bohr is used for all cases. The solid line shows the result of a reference calculation using the GS2 method with a step size of 0.02 amu$^{1/2}$ Bohr.

IRC calculation using the GS2 method with a numerical integration step size of 0.02 amu$^{1/2}$ Bohr. Figure 1 also includes results using GS2, Local Quadratic Approximation (LQA), EulerPC, and HPC integrators with a step size of 0.05 amu$^{1/2}$ Bohr. Although EulerPC and HPC agree with the reference profile near the TS, these curves exhibit significant deviations from the reference outside of $-1.5 \leq s \leq 2.0$ amu$^{1/2}$ Bohr.

In this report, we describe a critical enhancement to EulerPC and HPC methods that corrects errors in curvature profiles such as those observed in Figure 1 (section 2). This improvement does not increase the computational expense of either method. Section 3 begins with initial numerical examinations of the improved predictor−corrector integrators on an empirical surface, followed by a reconsideration of the HNC → HCN reaction using the enhanced predictor−corrector (PC) integration methods. Concluding remarks are given in section 4.

## 2. METHODS

We begin this section by defining the reaction path curvature vector. We then briefly outline the EulerPC and HPC integrators as previously implemented. Readers interested in a complete description of these methods should consult the original papers.[28−31] Last, we describe enhancements to EulerPC and HPC necessary for correcting the errors observed in Figure 1.

**2.1. Reaction Path Curvature.** Expanding in the reaction coordinate $s$, the reaction path is given by

$$\mathbf{x}(s) = \mathbf{x}(0) + \mathbf{v}^0(0)s + \frac{1}{2}\mathbf{v}^1(0)s^2 + \ldots \tag{2}$$

where $\mathbf{v}^0$ and $\mathbf{v}^1$ are the reaction path tangent and curvature, respectively. The first-order term, $\mathbf{v}^0$, is defined as

$$\mathbf{v}^0(s) = \frac{d\mathbf{x}(s)}{ds} \tag{3}$$

and the second-order term is given by

$$\mathbf{v}^1(s) = \frac{d^2\mathbf{x}(s)}{ds^2} \tag{4}$$

The path tangent and curvature can also be written in terms of energy derivatives. The tangent, which is equivalent to the steepest descent expression of eq 1, can be expressed in terms of the energy first derivative

$$\mathbf{v}^0(s) = \frac{d\mathbf{x}}{ds} = -\frac{\mathbf{g}(\mathbf{x})}{|\mathbf{g}(\mathbf{x})|} \tag{5}$$

The reaction path curvature depends on the energy second derivatives

$$\mathbf{v}^1(s) = -\frac{\mathbf{H}\mathbf{v}^0 - (\mathbf{v}^{0t}\mathbf{H}\mathbf{v}^0)\mathbf{v}^0}{|\mathbf{g}(\mathbf{x})|} \tag{6}$$

where $\mathbf{H}$ is the second derivative, or Hessian, matrix ($H_{ij} = (\partial^2 E)/(\partial x_i \partial x_j)$).

If the magnitude of the energy gradient approaches zero, as is the case in the neighborhood of PES stationary points such as the TS, both the tangent and curvature expressions become ill-defined. At the TS, the tangent is given by the transition vector (the Hessian eigenvector corresponding to the imaginary frequency), and the curvature vector is given by

$$\mathbf{v}^1(s) = -[\mathbf{H} - 2(\mathbf{v}^{0t}\mathbf{H}\mathbf{v}^0)\mathbf{I}]^{-1}[\mathbf{F}^1\mathbf{v}^0 - (\mathbf{v}^{0t}\mathbf{F}^1\mathbf{v}^0)\mathbf{v}^0] \tag{7}$$

In eq 7, $\mathbf{I}$ is the identity matrix ($I_{ij} = \delta_{ij}$) and $\mathbf{F}^1$ is a projection of the energy third derivatives ($F_{ijk} = (\partial^3 E)/(\partial x_i \partial x_j \partial x_k)$) onto the reaction path tangent

$$F^1_{ij} = \sum_k F_{ijk} v^0_k \tag{8}$$

Because the curvature vector depends on the second-order change in the reaction pathway, it is especially sensitive to slight errors in the IRC integration.

**2.2. EulerPC and HPC Reaction Path Following Integrators.** Three basic computational steps are joined to make up PC integrators: a predictor integration step (P), one or more function evaluation steps (E), and a corrector integration step (C). EulerPC and HPC reaction path following integrators employ a P−E−C sequence. After a sizable P integration step is taken, the PES and its derivative(s) are evaluated (an E step). Using information from this E step and the previous integration step (the initiation point for the current P step), a local fitted surface is constructed, and a highly accurate C step integration is carried out.

For EulerPC, the P component makes use of first-order Euler integration; HPC makes use of the second-order LQA integrator of Page and McIver.[15,16] The surface fitting and corrector integration for EulerPC and HPC are carried out using the same approaches. The corrector integration scheme is the modified Bulirsch−Stoer method.[28,45−47] The local surface fitting is done using modified-Shepard interpolation, or distance weighted interpolants (DWI).[48,49] These surfaces are written as weighted linear combinations of Taylor series expansions about the two input data points

$$E_{\mathrm{DWI}}(\mathbf{x}) = w_{i-1}(\mathbf{x})T_{i-1}(\mathbf{x}) + w_{\tilde{i}}(\mathbf{x})T_{\tilde{i}}(\mathbf{x}) \tag{9}$$

where $w$ and $T$ are the weighting functions and Taylor expansions. Subscripts $i-1$ and $\tilde{i}$ indicate the previous step's end point and the current P end point, respectively.

In previous implementations of these two integrators,[28−31] the DWI weighting functions have been given by

$$w_{i-1} = \frac{|\Delta\mathbf{x}_{\tilde{i}}|^2}{|\Delta\mathbf{x}_{i-1}|^2 + |\Delta\mathbf{x}_{\tilde{i}}|^2}$$

$$w_{\tilde{i}} = \frac{|\Delta\mathbf{x}_{x-1}|^2}{|\Delta\mathbf{x}_{i-1}|^2 + |\Delta\mathbf{x}_{\tilde{i}}|^2} \tag{10}$$

where $\Delta\mathbf{x}_{i-1} = \mathbf{x} - \mathbf{x}_{i-1}$ and $\Delta\mathbf{x}_{\tilde{i}} = \mathbf{x} - \tilde{\mathbf{x}}_i$. Note that the weights given in eq 10 are normalized and correspond to *primitive* (pre-normalization) weights of $|\Delta x|^{-2}$. The Taylor expansions are given by

$$\begin{aligned} T_{i-1}(\mathbf{x}) &= E_{i-1} + \mathbf{g}_{i-1}^t\Delta\mathbf{x}_{i-1} + \frac{1}{2}\Delta\mathbf{x}_{i-1}^t\mathbf{H}_{i-1}\Delta\mathbf{x}_{i-1} \\ T_{\tilde{i}}(\mathbf{x}) &= E_{\tilde{i}} + \mathbf{g}_{\tilde{i}}^t\Delta\mathbf{x}_{\tilde{i}} + \frac{1}{2}\Delta\mathbf{x}_{\tilde{i}}^t\mathbf{H}_{\tilde{i}}\Delta\mathbf{x}_{\tilde{i}} \end{aligned} \tag{11}$$

$E$, $\mathbf{g}$, and $\mathbf{H}$ are the energy, gradient, and Hessian at the points indicated by each term's subscript.

**2.3. Improved EulerPC and HPC Integrators.** An interesting observation from Figure 1 is that EulerPC and HPC yield essentially identical erroneous scalar curvature profiles. In previous studies, it has been shown that while the P integration steps can be quite different for these two methods, the robust corrector integration scheme tends to put both integrators onto the same solution pathway.[30,32] We, therefore, hypothesized that the source of the errors in scalar curvature stems from a deficiency in the DWI fitted surface. Again, the reaction path curvature is sensitive to rapid changes in the energy second derivatives along the reaction path, especially in regions where the energy gradient is small. This is obvious from the curvature expression at the TS, where the gradient is zero. As shown in eq 7, the curvature is explicitly dependent on the projection of the energy third derivatives onto the reaction coordinate.

The corrector integrator can only be as accurate as the DWI representation of the PES, which we determined to be the source of the PC based curvature errors observed in Figure 1. It is known that a DWI surface becomes exact to $n$th order if two conditions are met.[50] First, the primitive weighting functions must decay as $|\Delta x|^{-(n+1)}$. Second, the Taylor expansions must include the $n$th order contribution. Since EulerPC and HPC implementations used in all previous works employed weights that go as $|\Delta x|^{-2}$ and Taylor expansions truncated at second-order, it seemed that modifications to both aspects of the DWI fitting procedure would be necessary to achieve accurate scalar curvature profiles. Therefore, we propose two improvements to these PC integrators, which throughout the remainder of this work will be referred to as *enhanced* or *improved* EulerPC and HPC methods.

The two necessary enhancements have been incorporated by generalizing our DWI surface fitting program. One generalization has been to allow any primitive weighting function of the form $|\Delta x|^{-p}$. The results shown in the following section have been obtained with $p = 4$, which is a sufficient value to ensure that the DWI weighting functions preserve third-order accuracy. Because evaluation of the full set of third derivatives becomes prohibitively expensive with system size when using electronic structure methods (whether computed analytically or numerically), the Taylor series expansions have been modified to include only third-order terms on the line between the two input data points, $\mathbf{x}_{i-1}$ and $\tilde{\mathbf{x}}_i$. This simplification is reasonable since the curvature does not directly depend on the third-order structure perpendicular to the reaction path. Furthermore, we apply the sensible approximation that the energy third derivatives along this line are constant and, thus, both $T_{i-1}$ and $T_{\tilde{i}}$ include the same third derivatives. Now, the Taylor expansions used in DWI fits using the improved methods are

$$\begin{aligned} T_{i-1}(\mathbf{x}) &= E_{i-1} + \mathbf{g}_{i-1}^t\Delta\mathbf{x}_{i-1} + \frac{1}{2}\Delta\mathbf{x}_{i-1}^t\mathbf{H}_{i-1}\Delta\mathbf{x}_{i-1} \\ &\quad + \frac{1}{6}(\Delta\mathbf{x}_{i-1}^t\mathbf{f})\Delta\mathbf{x}_{i-1}^t\bar{\mathbf{F}}\Delta\mathbf{x}_{i-1} \\ T_{\tilde{i}}(\mathbf{x}) &= E_{\tilde{i}} + \mathbf{g}_{\tilde{i}}^t\Delta\mathbf{x}_{\tilde{i}} + \frac{1}{2}\Delta\mathbf{x}_{\tilde{i}}^t\mathbf{H}_{\tilde{i}}\Delta\mathbf{x}_{\tilde{i}} \\ &\quad + \frac{1}{6}(\Delta\mathbf{x}_{\tilde{i}}^t\mathbf{f})\Delta\mathbf{x}_{\tilde{i}}^t\bar{\mathbf{F}}\Delta\mathbf{x}_{\tilde{i}} \end{aligned} \tag{12}$$

where the matrix $\bar{\mathbf{F}}$ is

$$\bar{\mathbf{F}} = \left(\frac{1}{|\mathbf{x}_{\tilde{i}} - \mathbf{x}_{i-1}|}\right)(\mathbf{H}_{\tilde{i}} - \mathbf{H}_{i-1}) \tag{13}$$

and the vector $\mathbf{f}$ is

$$\mathbf{f} = \frac{\mathbf{x}_{\tilde{i}} - \mathbf{x}_{i-1}}{|\mathbf{x}_{\tilde{i}} - \mathbf{x}_{i-1}|} \tag{14}$$

Importantly, adding the approximate third-order term in eq 12 does not affect CPU or memory scalings for DWI evaluations. The scaling for both cost metrics remains $O(N_a^2)$ (where $N_a$ is the number of atomic centers).

## 3. RESULTS AND DISCUSSION

To examine the performance of the EulerPC and HPC integrators described in the previous section, two test cases have been chosen. We begin this section considering a model PES. Then, we return to the HCN rearrangement reaction from the Introduction to determine if the improved EulerPC and HPC integrators are able to accurately produce the scalar curvature profile. Electronic structure, geometry optimization, and IRC calculations have been carried out using a local development version of the Gaussian program suite.[51] The URVA analysis was done with the URVA program.[52]

**3.1. Two-Dimensional PES Model.** The first test case studied is the two-dimensional model given by

$$E(x, y) = \operatorname{arccot}\left[-e^y \cot\left(\frac{x}{2} - \frac{\pi}{4}\right)\right] - 2e^{-(y-\sin x)^2/2} \tag{15}$$

As pointed out in other work,[23] this surface is useful for testing reaction path integrators, particularly when considering path curvature. Both the IRC solution and the reaction path curvature can be determined analytically. The IRC is given by

$$y = \sin x \tag{16}$$

and the curvature is

$$\kappa^2 = \sin^2\left[\frac{x}{(1 + \cos^2 x)^3}\right] \tag{17}$$

Plots of the scalar curvature on this surface using GS2, LQA, EulerPC, and HPC integrators are shown in Figure 2. Three different integration step sizes have been considered: 0.2, 0.4, and 0.6. For all cases, the reaction path integration was initialized at $(-\pi,0)$ and terminated when the reaction coordinate reached $s = 7.640$, which corresponds to $(\pi,0)$ when the analytic path is followed.

In agreement with previous work by Gonzalez and Schlegel,[23] it is clear that LQA has difficulty following the reaction path well enough to accurately map the scalar curvature profile. With the smallest step size considered, the curve in Figure 2 exhibits artificial curvature minima and

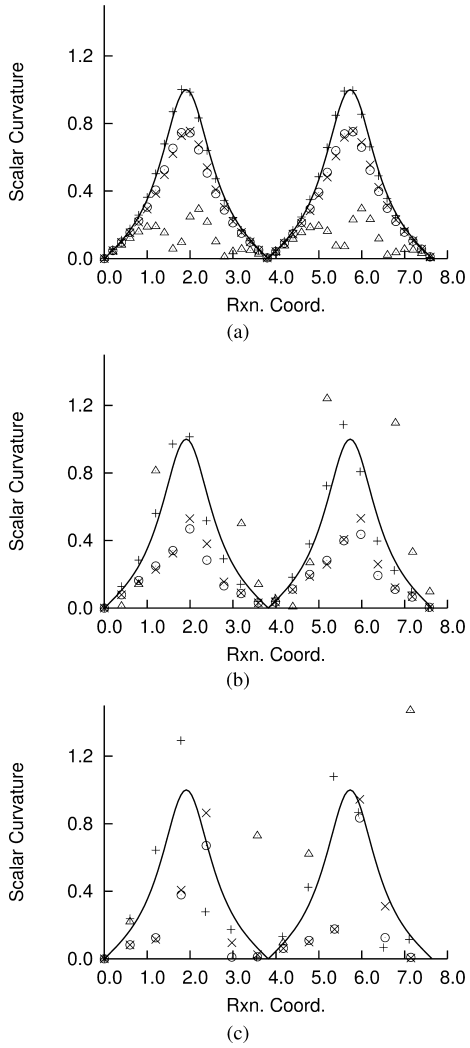


**Figure 2.** The scalar curvature as a function of reaction coordinate on the model surface given by eq 15 comparing GS2 (+), LQA (Δ), EulerPC (×), and HPC (○) integration methods. Numerical integration step sizes of (a) 0.20, (b) 0.40, and (c) 0.60 are shown. The analytic solution is given by the solid line.

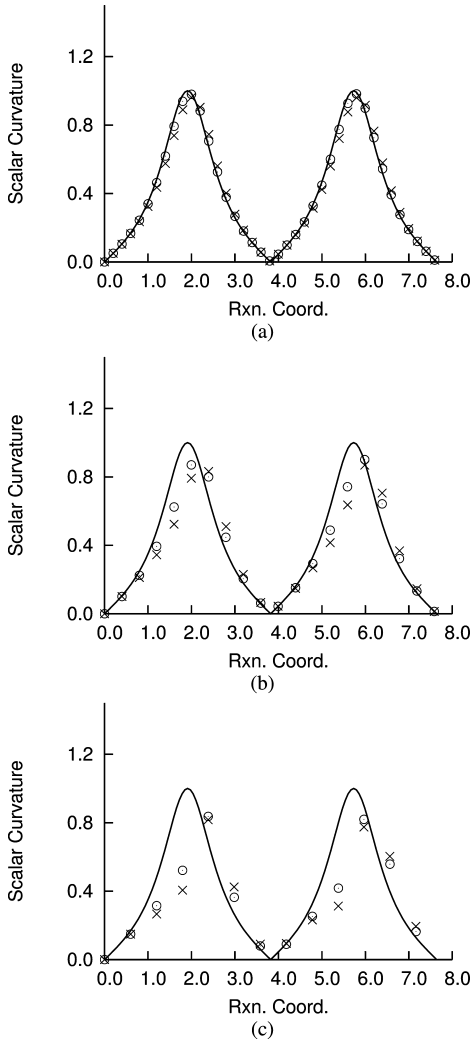


**Figure 3.** The scalar curvature as a function of reaction coordinate on the model surface given by eq 15 using the *enhanced* EulerPC (×) and HPC (○) reaction path integration methods. Numerical integration step sizes of (a) 0.20, (b) 0.40, (c) and 0.60 are shown. The analytic solution is given by the solid line.

significantly underestimates the maxima. Using either of the larger integration steps, the curvature profile wildly overestimates the maxima. Indeed, the maximum in the range of the path included in these tests is 3.9 (the analytic maximum scalar curvature is 1.0). The GS2 method is much better behaved and appears to give qualitatively correct curvature profiles for all three step sizes shown. However, with the largest step of $\Delta s$ = 0.60, the maxima are still overestimated by more than 25%.

As compared with GS2 and LQA, results using EulerPC and HPC shown in Figure 2 are quite similar to those observed in Figure 1. First, HPC performs better than LQA. This is expected since HPC is necessarily designed to *correct* LQA errors. Second, neither PC scheme performs as well as GS2. Third, the EulerPC profile is essentially identical to the HPC curve, which, again, suggests that remaining integration errors are likely due to limitations of the corrector integration component that is common to both PC methods.

The reaction path integrations on this surface were also carried out using the enhanced EulerPC and HPC methods proposed in section 2. Scalar curvature profiles from those calculations are shown in Figure 3. As before, reaction path integrations were carried out using step sizes of 0.2, 0.4, and 0.6. It is clear that the enhanced PC integrators provide a marked improvement over the original EulerPC and HPC methods. For $\Delta s$ = 0.20, scalar curvature profiles using enhanced EulerPC and HPC methods are in perfect agreement with the analytic solution of eq 17. Increasing the numerical integration step size leads to some degradation in the curvature results. Nevertheless, both enhanced PC approaches offer equivalent or better results compared with GS2. This is especially notable since GS2 involves an iterative solution (in practice by employing constrained optimizations) to solve each IRC step. In general, the number of PES evaluations required per integration point increases with step size. In contrast, the PC methods used here require only one PES evaluation per IRC point regardless of the numerical integration step size. The GS2 calculations shown in Figure 2 using a step size of 0.60 averaged 3.2 optimization cycles per IRC point.

Recently, it was shown that the quality of projected frequency reaction profiles using EulerPC and HPC integrators are essentially unaffected by Hessian updating.[32] Indeed, considering three different integration step sizes ($\Delta s$ = 0.04,

0.08, and 0.10 au) it was shown in that work that employing Hessian updating for as many as 10 IRC points between analytic Hessian and projected frequency evaluations yields results essentially identical to cases where analytic Hessians are computed at all IRC steps. With those results in mind, we have carried out an analogous series of tests in this study. Figure 4

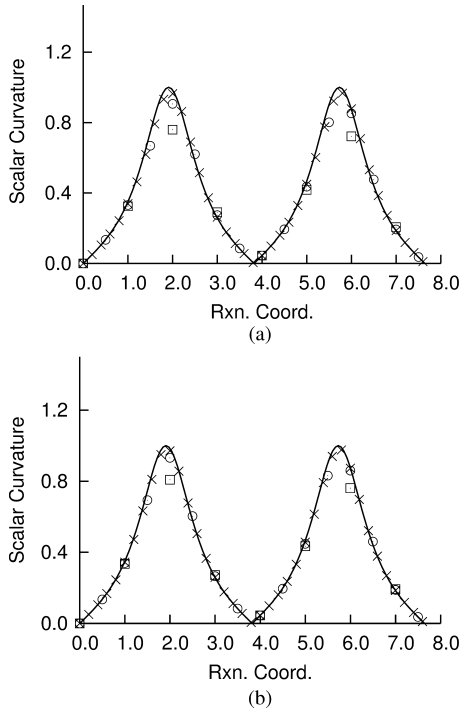


**Figure 4.** The scalar curvature as a function of reaction coordinate on the model surface given by eq 15 with analytic Hessians evaluated at all steps (solid line), every 2 (×), 5 (○), and 10 (□) integration steps using enhanced (a) EulerPC and (b) HPC integrators. An integration step size of 0.10 has been used in all cases.

compares the analytic curvature profile with enhanced EulerPC and HPC results using a numerical integration step size of 0.10 and analytic second derivatives evaluated every two, five, and 10 steps. Bofill's scheme[53] has been used to update the Hessian matrix at intermediate steps. With this step size, the calculation with analytic Hessians every other step results in the same number of second-derivative evaluations along the reaction path as the $\Delta s$ = 0.20 case shown in Figure 3. It is clear from Figure 4 that with Hessian updating these two PC integrators still provide a rather accurate description of the scalar curvature. Indeed, recalculating the Hessian every two or five steps does not yield any noticeable error in the scalar curvature profile. Even when the analytic Hessian evaluations are carried out only every 10 steps, the results are still in better agreement with the exact solution than those derived from $\Delta s$ = 0.4 paths using analytic Hessians at all steps (Figure 3).

**3.2. HCN Isomerization Reaction.** Having established that the PC integration enhancements introduced in this work correct observed errors in scalar curvature profiles on a model potential surface, we applied these methods to the HCN rearrangement reaction. As discussed in the Introduction, the curvature profiles given by EulerPC and HPC integration methods both exhibit substantial qualitative and quantitative errors (see Figure 1). Figure 5 shows scalar curvature plots for this reaction using enhanced EulerPC and HPC integrators

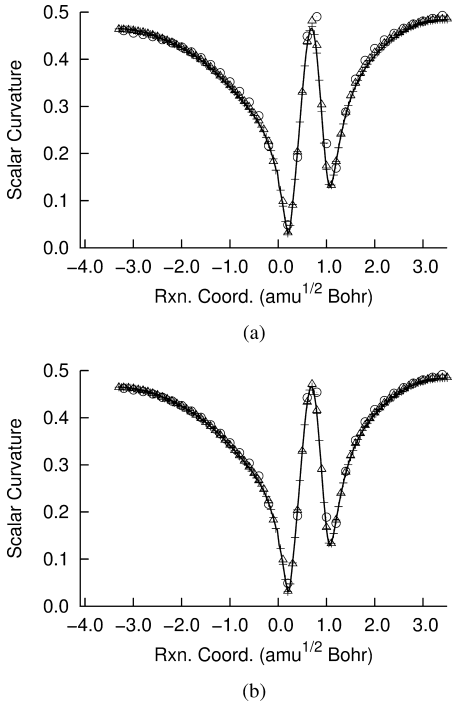


**Figure 5.** The scalar curvature as a function of reaction coordinate for the HCN → HNC rearrangement reaction using enhanced (a) EulerPC and (b) HPC integrators with numerical integration step sizes of 0.05 (+), 0.10 (Δ), and 0.20 (○) amu$^{1/2}$ Bohr.

with numerical integration step sizes of 0.05, 0.10, and 0.20 amu$^{1/2}$ Bohr. For comparison, the GS2 results (using a step size of 0.02 amu$^{1/2}$ Bohr) are also shown. With the larger two step sizes considered, the EulerPC curve slightly overshoots the maximum around $\Delta s$ = −0.7 amu$^{1/2}$ Bohr. Also, the $\Delta s$ = 0.20 amu$^{1/2}$ Bohr HPC path begins to deviate from the reference solution when approaching the reactant well. Otherwise, the agreement with GS2 is excellent.

The curvature along the reaction path for this reaction has also been evaluated by using analytic Hessians every 2, 5, or 10 IRC points; intermediate integration steps made use of Hessian updating.[53] The path curvature has been determined only at points where analytic Hessians are available. Results of these calculations are shown in Figure 6. Curvature profiles for these three cases display near perfect agreement with the all-analytic Hessian results in the region near the TS. As the IRC heads into reactant and product PES minima, Hessian updating introduces some errors in the scalar curvature profiles. It is interesting to note that these observed errors occur in regions where the path exhibits large curvature. Because Hessian updating methods numerically determine changes in the second-derivative matrix in one or two dimensions at a time, the quality of these schemes will necessarily be compromised when stepping along extended portions of a pathway with large curvature. Still, the error in the scalar curvature at the two ends of the reaction path are relatively small, with a maximum relative error of roughly 10% around $s$ = −3.3 Bohr amu$^{1/2}$. Certainly, reaction path curvature calculations using periodic Hessian updating for initial exploratory studies may be a useful technique given the significant cost savings associated with updating for sizable electronic structure studies. Another possible suggestion one might take away from the results in Figure 6 relates to developing automated approaches for determining when Hessian updating can safely be employed in

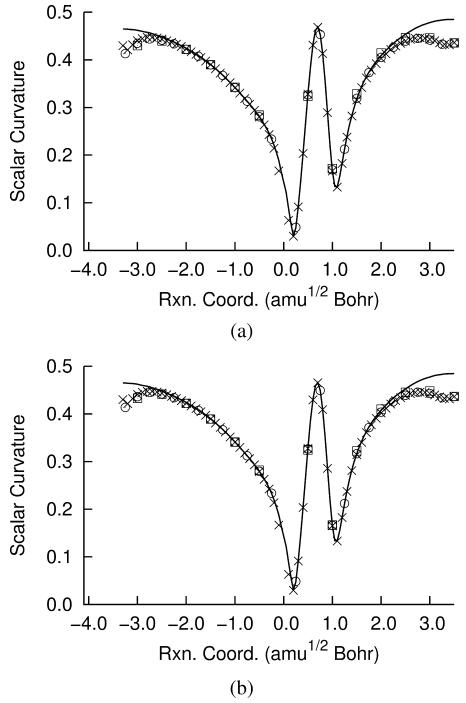


**Figure 6.** The scalar curvature as a function of reaction coordinate for the HCN → HNC rearrangement reaction with analytic Hessians evaluated at all steps (solid line), every 2 (×), 5 (○), and 10 (□) integration steps using enhanced (a) EulerPC and (b) HPC integrators. An integration step size of 0.05 amu$^{1/2}$ Bohr has been used in all cases.

reaction path calculations. One possibility may be to use Hessian updating in regions of the path where small curvature is detected and to employ full analytic Hessian evaluations in regions of the path where the curvature is large or rapidly changing. Automated Hessian updating schemes of this sort may be explored in future studies.

A key feature of URVA is the analysis of the reaction path curvature. The electronic structure changes of the reaction complex are reflected by the scalar path curvature plotted as a function of $s$. Curvature minima ($M_n$) correspond to minimal transient structures with minimal changes whereas curvature maxima ($K_m$) describe the chemical processes, such as bond breaking/forming, rehybridization, etc.[37−39,54] In this way, meaningful checkpoints along a chemical reaction path are obtained that can be used to unravel the mechanism of a chemical reaction. The curvature minima $M_n$ can be used to partition the reaction into reaction phases, which stretch from one curvature minimum to the next and enclose a curvature maximum or enhancement representing a particular change of the reaction complex. Different types of chemical reactions possess a different curvature pattern, which can be used as the fingerprint of the reaction. Further details can be gained by a decomposition of the scalar reaction path curvature into normal mode curvature coupling coefficients $B_{n,s}$ and a decomposition in terms of local mode curvature coupling coefficients $A_{k,s}$.[37−39,54] Both the scalar curvature as well as the normal and local mode curvature coupling coefficients are sensitive to inaccuracies of the reaction path caused by deficiencies of the integrator used. As discussed above, this is particularly true in the vicinity of stationary points where the energy gradient $\mathbf{g}(\mathbf{x})$ approaches zero and eqs 5 and 6 become ill-defined.

For many chemical reactions, such as addition reactions of the type $XH_n + H_2$,[55] the scalar curvature in both the entrance and exit channels is negligibly small because these regions are dominated by van der Waals interactions. Therefore, inaccuracies in the reaction path curvature do not play a major role, and GS2, HPC, and EulerPC methods lead to the same results.[55] However, in the case of rearrangement reactions (such as carbene rearrangements) or rotations about multiple bonds (such as ethylene, allene), which involve major rehybridization right from the start, the curvature in entrance and exit channels is large and, therefore, is strongly affected by path inaccuracies. The same is true for isomerization reactions starting from a linear arrangement such as the HCN isomerization. An infinitesimal bending of the reactant leads to a sudden change in symmetry, which causes a large reaction path curvature in the entrance channel. The same is true for the reverse reaction.

The HCN reaction complex ($C_s$ symmetry) possesses two vibrational modes orthogonal to the reaction path. In Figure 7, the scalar reaction path curvature and its decomposition into local mode coupling coefficients $B_{1,s}$ and $B_{2,s}$ are shown as a function of $s$. Figure 7a results are based on the HPC integrator, and Figure 7b results are based on the enhanced HPC integrator. In Figure 7c, the differences between both methods are given. As is obvious from Figure 7c, large differences occur in regions of small energy gradient $\mathbf{g}(\mathbf{x})$, around the TS, in the entrance channel, and most strongly in the exit channel. Applying the HPC integrator the curvature rises in the entrance channel from a zero value at $s = -3.4$ amu$^{1/2}$ Bohr within two $s$ units to a value of 0.43 amu$^{-1/2}$ Bohr$^{-1}$. In the exit channel, the curvature first drops down to a third transient point M3 at $s =$ 3.9 amu$^{1/2}$ Bohr$^{-1}$ and rises steeply within the next two $s$ units reaching the end of the exit channel. The transient points M1 and M2 correspond to nonclassical structures of the reaction complex, separated by the curvature maximum K2, while M3 seems to be an artifact of the integrator rather than the starting point of another reaction phase (see Figure 8). Comparison with the GS2 and the enhanced HPC integrator results (Figure 7b) clearly confirms this. It is noteworthy that $B_{2,s}$ is more affected than $B_{1,s}$. In Figure 9, the harmonic frequencies $\omega_1$ and $\omega_2$ are shown as a function of $s$. Both HPC and enhanced HPC give the same results, which confirms that only properties depending on energy third derivative information along the reaction path are affected by path inaccuracies. Obviously, changes of $\omega_2$ along $s$ are much larger than those of $\omega_1$. $\omega_2$ couples more strongly with the reaction path than $\omega_1$ and, as a consequence, displays much stronger the reaction path inaccuracies. In summary, the TS region, entrance, and exit channel of the HCN isomerization are described correctly with the enhanced HPC integrator. In particular, there is no artificial transient point M3 leading to a fourth reaction phase without any chemical relevance.

## 4. CONCLUSIONS

The possibility of using EulerPC or HPC reaction path following integrators for evaluating scalar curvature profiles has been investigated. Despite the success of these methods for finding projected frequency profiles, it has been shown here that both PC schemes give pathways that yield scalar curvature profiles with large quantitative and qualitative errors. We have identified the source of this failure and proposed improvements that do not change the formal scaling of CPU or memory cost metrics. The enhanced EulerPC and HPC integrators have

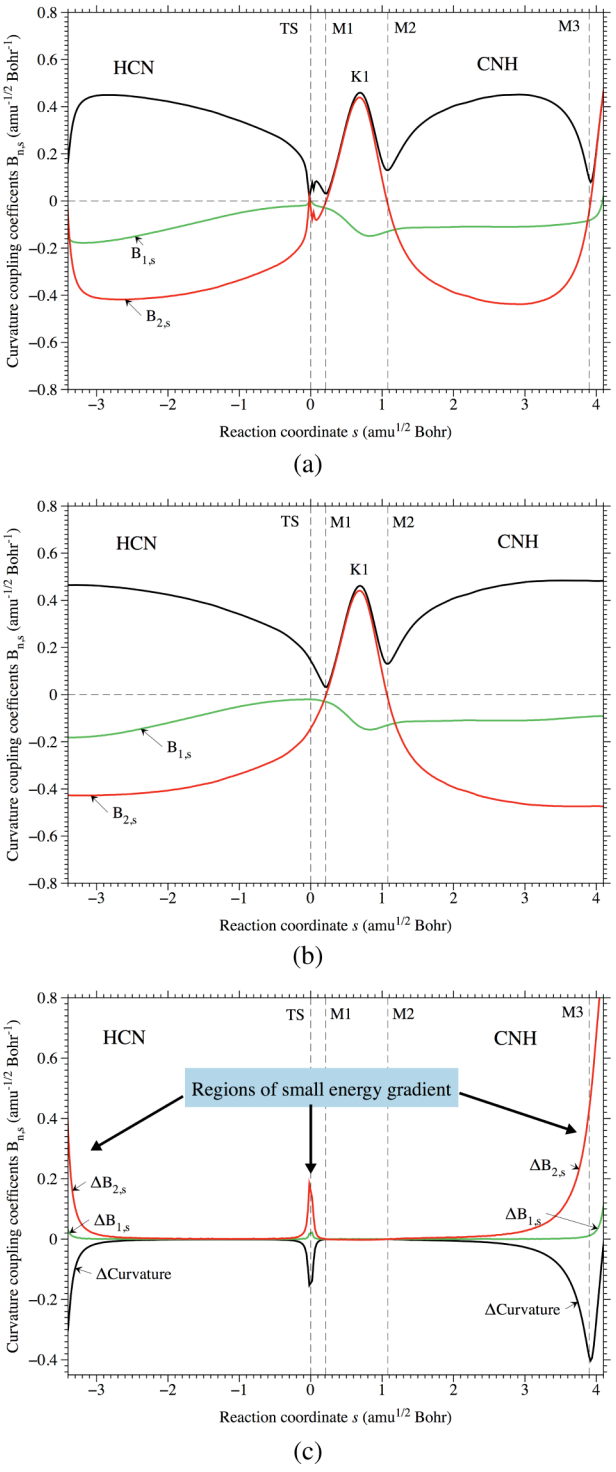


**Figure 7.** Decomposition of the scalar reaction path curvature (bold black line) of the HCN → HNC rearrangement reaction in terms of normal mode curvature coupling coefficients $B_{n,s}(s)$ (colored lines). Vertical dashed lines separate the reaction phases. The position of the transition state corresponds to $s$ = 0 amu$^{1/2}$ Bohr; (a) using the HPC integrator, (b) using the enhanced HCP integrator with a numerical integration step size of 0.05 amu$^{1/2}$ Bohr; (c) differences between both methods. B3LYP/6-31G(d,p) calculations.

been tested with an analytic two-dimensional model surface and a chemical reaction studied with the B3LYP/6-31G(d,p) model chemistry. For both test systems, the enhanced PC integrators developed in this work perform extremely well.

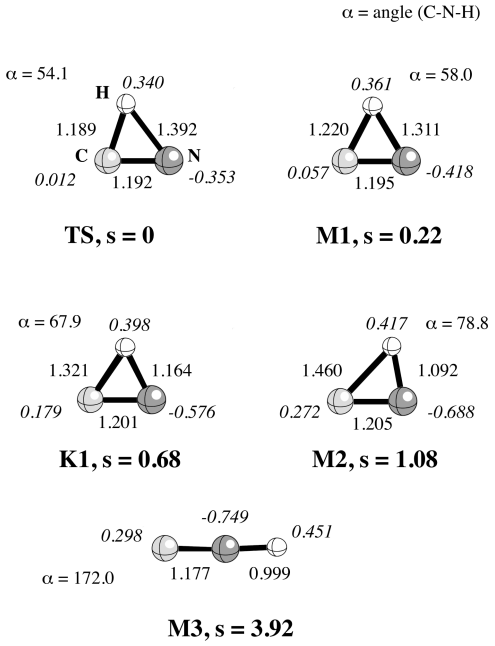


**Figure 8.** Geometries (normal print) and NBO charges[56,57] (italics) of the HCN → HNC rearrangement reaction complex at the transition state TS, curvature minima M1−M3, and curvature maximum K1 using the HPC integrator with a numerical integration step size of 0.02 amu$^{1/2}$ Bohr; bond lengths in Å, bond angles in degree, charges in electron, B3LYP/6-31G(d,p) calculations.

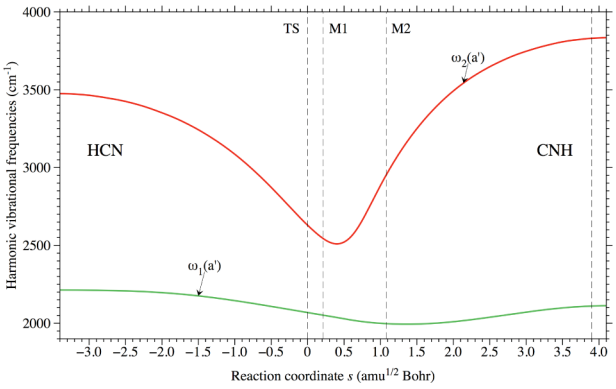


**Figure 9.** Harmonic vibrational frequencies $\omega_n$ as a function of the reaction coordinate. Vertical dashed lines separate the reaction phases. The position of the transition state corresponds to $s$ = 0 amu$^{1/2}$ Bohr. B3LYP/6-31G(d,p) calculations.

The use of Hessian updating between periodic analytic second-derivative evaluations, as an approach to decrease the overall cost of IRC calculations using electronic structure methods, has also been explored. It appears that such a scheme works quite well with the improved EulerPC and HPC methods. However, in regions of the reaction pathway where the magnitude of the curvature remains large for some length of the reaction coordinate, Hessian updating appears to degrade the quality of the IRC. In these regions, it may be necessary to analytically evaluate the Hessian with greater frequency, perhaps at every integration step. In future work, these integrators will be used to explore chemical reaction mechanisms with the URVA and other related methods.


dx.doi.org/10.1021/ct301021y | J. Chem. Theory Comput. 2013, 9, 1481−1488

## AUTHOR INFORMATION


### Corresponding Author

*E-mail: hrant@gaussian.com; ekraka@smu.edu.


### Notes

The authors declare no competing financial interest.

## ACKNOWLEDGMENTS

Prof. H. B. Schlegel (Wayne State University) is thanked for helpful discussions. E.K. thanks the NSF for financial support, Grant No. CHE 1152357.

## REFERENCES


(1) Eyring, H. *J. Chem. Phys.* **1935**, *3*, 107.
(2) Evans, M. G.; Polanyi, M. *Trans. Faraday Soc.* **1935**, *31*, 875.
(3) Fukui, K. *Acc. Chem. Res.* **1981**, *14*, 363−368.
(4) Schlegel, H. B. *WIREs Comput. Mol. Sci.* **2011**, *1*, 790−809.
(5) Hratchian, H. P.; Schlegel, H. B. In *Theory and Applications of Computational Chemistry: The First Forty Years*; Dykstra, C. E., Frenking, G., Kim, K. S., Scuseria, G. E., Eds.; Elsevier: Amsterdam, 2005; pp 195−249.
(6) Schlegel, H. B. *J. Comput. Chem.* **2003**, *24*, 1514−1527.
(7) Wales, D. J. *Energy Landscapes*; Cambridge University Press: Cambridge, U. K., 2003.
(8) Schlegel, H. B. In *Encyclopedia of Computational Chemistry*; Schleyer, P. v. R., Allinger, N. L., Kollman, P. A., Clark, T., Schaefer Iii, H. F., Gasteiger, J., Schreiner, P. R., Eds.; Wiley: Chichester, U. K., 1998; Vol. *4*, pp 2432−2437.
(9) Collins, M. A. *Adv. Chem. Phys.* **1996**, *93*, 389−453.
(10) Schmidt, M. W.; Gordon, M. S.; Dupuis, M. *J. Am. Chem. Soc.* **1985**, *107*, 2585−2589.
(11) Ishida, K.; Morokuma, K.; Komornicki, A. *J. Chem. Phys.* **1977**, *66*, 2153−2156.
(12) Baldridge, K. K.; Gordon, M. S.; Steckler, R.; Truhlar, D. G. *J. Phys. Chem.* **1989**, *93*, 5107−5119.
(13) Garrett, B. C.; Redmon, M. J.; Steckler, R.; Truhlar, D. G.; Baldridge, K. K.; Bartol, D.; Schmidt, M. W.; Gordon, M. S. *J. Phys. Chem.* **1988**, *92*, 1476−1488.
(14) Aguilar-Mogas, A.; Gimenez, X.; Bofill, J. M. *Chem. Phys. Lett.* **2006**, *432*, 375−382.
(15) Page, M.; McIver, J. M. *J. Chem. Phys.* **1988**, *88*, 922−935.
(16) Page, M.; Doubleday, C.; McIver, J. W. *J. Chem. Phys.* **1990**, *93*, 5634−5642.
(17) Sun, J. Q.; Ruedenberg, K. *J. Chem. Phys.* **1993**, *99*, 5257−5268.
(18) Sun, J. Q.; Ruedenberg, K. *J. Chem. Phys.* **1993**, *99*, 5269−5275.
(19) Eckert, F.; Werner, H. J. *Theor. Chem. Acc.* **1998**, *100*, 21−30.
(20) Maluendes, S. A.; Dupuis, M. J. *J. Chem. Phys.* **1990**, *93*, 5902−5911.
(21) Hratchian, H. P.; Schlegel, H. B. *J. Phys. Chem. A* **2002**, *106*, 165−169.
(22) Müller, K.; Brown, L. D. *Theor. Chim. Acta* **1979**, *53*, 75−93.
(23) Gonzalez, C.; Schlegel, H. B. *J. Chem. Phys.* **1991**, *95*, 5853−5860.
(24) Gonzalez, C.; Schlegel, H. B. *J. Chem. Phys.* **1989**, *90*, 2154−2161.
(25) Gonzalez, C.; Schlegel, H. B. *J. Phys. Chem.* **1990**, *94*, 5523−5527.
(26) Burger, S. K.; Yang, W. T. *J. Chem. Phys.* **2006**, *124*, 224102.
(27) Burger, S. K.; Yang, W. T. *J. Chem. Phys.* **2006**, *125*, 244108.
(28) Hratchian, H. P.; Schlegel, H. B. *J. Chem. Phys.* **2004**, *120*, 9918−9924.
(29) Hratchian, H. P.; Schlegel, H. B. *J. Chem. Theory Comput.* **2005**, *1*, 61−69.
(30) Hratchian, H. P.; Frisch, M. J.; Schlegel, H. B. *J. Chem. Phys.* **2010**, *133*, 224101.
(31) Hratchian, H. P.; Frisch, M. J. *J. Chem. Phys.* **2011**, *134*, 204103.
(32) Hratchian, H. P. *J. Chem. Theory Comput.* **2012**, *8*, 5013−5019.
(33) Garrett, B. C.; Truhlar, D. G. In *Encyclopedia of Computational Chemistry*; Schleyer, P. v. R., Allinger, N. L., Kollman, P. A., Clark, T., Schaefer, H. F., III, Gasteiger, J., Schreiner, P. R., Eds.; Wiley: Chichester, U. K., 1998; Vol. *2*, pp 3094−3104.
(34) Truhlar, D. G.; Garrett, B. C.; Klippenstein, S. J. *J. Phys. Chem.* **1996**, *100*, 12771−12800.
(35) Truhlar, D. G.; Garrett, B. C. *Annu. Rev. Phys. Chem.* **1984**, *35*, 159−189.
(36) Miller, W. H.; Handy, N. C.; Adams, J. E. *J. Chem. Phys.* **1980**, *72*, 99−112.
(37) Kraka, E. *WIREs Comput. Mol. Sci.* **2011**, *1*, 531−556.
(38) Kraka, E.; Cremer, D. *Acc. Chem. Res.* **2010**, *43*, 591−601.
(39) Kraka, E. In *Encyclopedia of Computational Chemistry*; Schleyer, P. v. R., Allinger, N. L., Kollman, P. A., Clark, T., Schaefer, H. F., III, Gasteiger, J., Schreiner, P. R., Eds.; Wiley: Chichester, U. K., 1998; Vol. *2*, pp 2437−2463.
(40) Becke, A. D. *Phys. Rev. A* **1988**, *38*, 3098.
(41) Becke, A. D. *J. Chem. Phys.* **1993**, *98*, 5648.
(42) Lee, C. T.; Yang, W. T.; Parr, R. G. *Phys. Rev. B* **1988**, *37*, 785−789.
(43) Stevens, J. P.; Devlin, F.; Chablowski, C.; Frisch, M. *J. Chem. Phys.* **1994**, *98*, 11623.
(44) Hariharan, P. C.; Pople, J. A. *Theor. Chim. Acta.* **1973**, *28*, 213.
(45) Bulirsch, R.; Stoer, J. *Num. Math.* **1964**, *6*, 413−427.
(46) Bulirsch, R.; Stoer, J. *Num. Math.* **1966**, *8*, 93−104.
(47) Bulirsch, R.; Stoer, J. *Num. Math.* **1966**, *8*, 1−13.
(48) Thompson, K. C.; Jordan, M. J. T.; Collins, M. A. *J. Chem. Phys.* **1998**, *108*, 564−578.
(49) Collins, M. A. *Theor. Chem. Acc.* **2002**, *108*, 313−324.
(50) Ischtwan, J.; Collins, M. A. *J. Chem. Phys.* **1994**, *100*, 8080−8088.
(51) Frisch, M. J.; Trucks, G. W.; Schlegel, H. B.; Scuseria, G. E.; Robb, M. A.; Cheeseman, J. R.; Scalmani, G.; Barone, V.; Mennucci, B.; Petersson, G. A.; Nakatsuji, H.; Caricato, M.; Li, X.; Hratchian, H. P.; Izmaylov, A. F.; Bloino, J.; Zheng, G.; Sonnenberg, J. L.; Liang, W.; Hada, M.; Ehara, M.; Toyota, K.; Fukuda, R.; Hasegawa, J.; Ishida, M.; Nakajima, T.; Honda, Y.; Kitao, O.; Nakai, H.; Vreven, T.; Montgomery, J. A., Jr.; Peralta, J. E.; Ogliaro, F.; Bearpark, M.; Heyd, J. J.; Brothers, E.; Kudin, K. N.; Staroverov, V. N.; Keith, T.; Kobayashi, R.; Normand, J.; Raghavachari, K.; Rendell, A.; Burant, J. C.; Iyengar, S. S.; Tomasi, J.; Cossi, M.; Rega, N.; Millam, J. M.; Klene, M.; Knox, J. E.; Cross, J. B.; Bakken, V.; Adamo, C.; Jaramillo, J.; Gomperts, R.; Stratmann, R. E.; Yazyev, O.; Austin, A. J.; Cammi, R.; Pomelli, C.; Ochterski, J. W.; Martin, R. L.; Morokuma, K.; Zakrzewski, V. G.; Voth, G. A.; Salvador, P.; Dannenberg, J. J.; Dapprich, S.; Parandekar, P. V.; Mayhall, N. J.; Daniels, A. D.; Farkas, O.; Foresman, J. B.; Ortiz, J. V.; Cioslowski, J.; Fox, D. J. *GAUSSIAN*, Development Version, Revision H.20+; Gaussian, Inc.: Wallingford, CT, 2012.
(52) Kraka, E.; Filatov, M.; Zou, W.; Grafenstein, J.; Izotov, D.; Gauss, J.; He, Y.; Wu, A.; Polo, V.; Cremer, D.; Olsson, L.; Konkoli, Z.; He, Z. *URVA2011*; Southern Methodist University: Dallas, TX, 2011.
(53) Bofill, J. M. *J. Comput. Chem.* **1994**, *15*, 1−11.
(54) Cremer, D.; Kraka, E. *Curr. Org. Chem.* **2010**, *14*, 1524−1560.
(55) Kraka, E.; Zou, W.; Freindorf, M.; Cremer, D. *J. Chem. Theory Comput.* **2012**, *8*, 4931−4943.
(56) Reed, A.; Curtiss, L.; Weinhold, F. *Chem. Rev.* **1988**, *88*, 899−926.
(57) Weinhold, F.; Landis, C. R. *Valency and Bonding: A Natural Bond Orbital Donor-Acceptor Perspective*; Cambridge University Press: Cambridge, U. K.; 2003.